View Online



# Probe dependence of spatially heterogeneous dynamics in supercooled glycerol as revealed by single molecule microscopy†

**Stephan A. Mackowiak, Lindsay M. Leone and Laura J. Kaufman***

*Received 18th September 2010, Accepted 29th October 2010*
**DOI: 10.1039/c0cp01860k**

Published on 26 November 2010 on http://pubs.rsc.org | doi:10.1039/C0CP01860K
Downloaded by Columbia University on 04 February 2011

Spatially heterogeneous dynamics in supercooled glycerol over the temperature range 198 K ($1.04T_g$) − 212 K ($1.12T_g$) is investigated using widefield single molecule (SM) fluorescence microscopy. Measurements are performed using three different perylenedicarboximide probes to investigate whether probe size and probe–host interactions affect breadth of heterogeneity reported in the glassy host by such SM experiments. Rotational relaxation times of single probe molecules are measured, and for all probes, log-normal distributions of relaxation times are found. No significant change in relaxation time distribution as a function of temperature is evident for a given probe. However, across probes, probe rotational relaxation time is correlated with breadth of heterogeneous dynamics reported. Molecules that undergo changes in dynamics are identified using two complementary approaches that interrogate time scales between $10^3$ and $10^6$ $\tau_\alpha$,with $\tau_\alpha$ the structural relaxation time of glycerol. Exchange is found on the shortest time scales probed ($\sim$30 $\tau_c$, with $\tau_c$ the rotational correlation time of the probe) and is relatively temperature and probe independent. No evidence is found for additional exchange occurring on the longest time scales interrogated. Taken together with the fact that probes that rotate the fastest report the greatest breadth of spatially heterogeneous dynamics in the system, this indicates that exchange times reported from analysis of SM linear dichroism trajectories as described here are upper bounds on the average exchange time in the system.

## I. Introduction

Amorphous systems lacking long range order in the temperature range between the melting temperature, $T_m$, and the glass transition temperature, $T_g$, are known as supercooled liquids. The non-exponential relaxations observed in such systems are consistent with the existence of spatially heterogeneous dynamics. Because it is natural for the single molecule (SM) experiment performed, we discuss spatially heterogeneous dynamics in terms of spatial heterogeneity and temporal heterogeneity. Spatial heterogeneity refers to the presence of distinct regions in the supercooled liquid, each exhibiting exponential relaxations, but with time constants that may differ significantly. Temporal heterogeneity refers to alterations in the dynamics of the system or a given spatial region within the system over time. In the widefield (WF) SM microscopy used in this study, heterogeneous dynamics can be identified by following dynamics of many single molecule probes in the same sample simultaneously. Breadth of relaxation times of such probes monitored over a given time reports on spatial heterogeneity. Explicit changes in particular molecules' dynamics over time report on temporal heterogeneity and may give direct access to exchange time, the average time over which an environment is characterized by a single relaxation time.

*Department of Chemistry, Columbia University, New York, NY 10027, USA. E-mail: kaufman@chem.columbia.edu*
† Electronic supplementary information (ESI) available: Description of heating correction procedure and demonstration of its use on dpPDI data. See DOI: 10.1039/c0cp01860k

Results from SM experiments on small organic molecule supercooled liquids to date have been largely consistent with each other in terms of reported spatial heterogeneity.[1–3] Most recently, two studies following probe molecule rotation in supercooled glycerol reached similar conclusions regarding the breadth of spatial heterogeneity present in the system. However, the two studies reached different conclusions regarding temporal heterogeneity.[2,3] In particular, in WF SM microscopy using rubrene as a probe in glycerol at $1.07T_g$, we reported that $\sim$15% of the molecules assessed experienced detectable changes in dynamics over the course of the experiment.[3] Of the molecules experiencing detected exchange, the average time until first exchange ($\tau_{pers}$) and the average time between exchanges ($\tau_{ex}$) were, respectively, $\sim$60 and 30 times the rotational correlation time of the rubrene probe, $\tau_c$. Given the rotational correlation time of rubrene relative to glycerol's structural or α-relaxation time ($\tau_\alpha$), these values translate to $\tau_{pers} \approx 400\ \tau_\alpha$ and $\tau_{ex} \approx 200\ \tau_\alpha$. In contrast, Zondervan *et al.* measured rotations of a perylenedicarboximide probe (*N*,*N*′-bis(2,5-di-*tert*-butylphenyl)-3,4,9,10-perylenedicarboximide, tbPDI) in glycerol and, over the temperature range of $1.08T_g$–$1.12T_g$, found evidence for very long-lived spatial heterogeneities, with almost all molecules exhibiting persistent rotational relaxation times and no dynamic exchange for $10^5$–$10^6$ $\tau_\alpha$.[2] This finding suggested a picture of supercooled glycerol as a mosaic of liquid-like regions separated by a nearly static network. The presence of such a network is not consistent with the picture of supercooled liquids as *ergodic*, *interchanging* mosaics of local environments[4] but was further supported by rheological findings and a study

 This journal is © the Owner Societies 2011

View Online

Published on 26 November 2010 on http://pubs.rsc.org | doi:10.1039/C0CP01860K
Downloaded by Columbia University on 04 February 2011

indicating fluorescent probes in supercooled glycerol are excluded from micron-size regions that may delineate the solid-like network.[5,6]

The discrepancy in measured exchange time relative to $\tau_\alpha$ in supercooled glycerol as revealed by the two SM microscopy experiments may emerge from a combination of factors. These include differences in probe size, probe–host interactions, sample preparation, and analysis methods. The probes used in the two studies were quite different in size and somewhat different in interactions with the host. The tbPDI used by Zondervan *et al*. is significantly larger (767 g mol$^{-1}$) and more structurally anisotropic than rubrene (532.7 g mol$^{-1}$), though both are significantly larger than glycerol (92 g mol$^{-1}$). Probes approaching the size of a region characterized by a single relaxation time in a system with spatial heterogeneity may sample and average over several distinct environments and thus fail to report the presence of the full breadth of spatial heterogeneity in the system (Fig. 1a). Just as large probe molecules may average over heterogeneities in space, they may also do so in time. Even in the presence of heterogeneous regions much larger than the probe, if the time scale for probe rotation is similar to or slower than the typical time over which a fast region of the supercooled liquid becomes slow or *vice versa*, the probe rotational relaxation times will not mirror the exchanges occurring in the environment (Fig. 1b). Both types of averaging over spatially heterogeneous dynamics in molecular glass formers have been considered previously,[7–10] though probe dependence studies have not yet been undertaken for single molecule approaches. Just as probe size may affect probe ability to report spatially heterogeneous dynamics in the host, interactions between probe and host molecules may do so as well. For example, a probe with strong interactions with the host may rotate with a shell or partial shell of host molecules, increasing the effective size of the probe. Another possibility is that non-polar probes may segregate into non-representative regions of a polar host or *vice versa* and in turn report preferentially on these regions of the supercooled host.

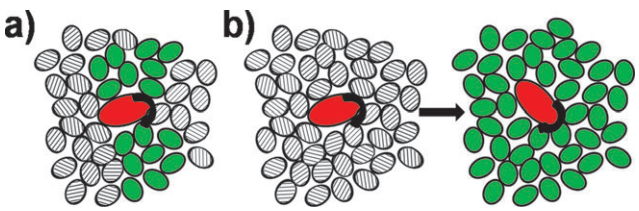


**Fig. 1** Schematic of a probe (red solid ellipsoid) in two different types of heterogeneous environments. (a) The probe is surrounded by two regions exhibiting different dynamics. Assuming the filled ellipsoids represent slow molecules and the striped ellipsoids represent fast molecules, if these regions maintain their dynamics for infinite time (*i.e*. there is spatial but not temporal heterogeneity in the system), a large probe will rotate through both types of regions, reporting an average dynamics. (b) If all molecules surrounding the probe are fast but become slow during the probe rotation (*i.e*. there is temporal heterogeneity but no spatial heterogeneity in the microenvironment of the probe), the probe will also only report an average dynamics. In the presence of both spatial and temporal heterogeneity, the probe may average over spatially heterogeneous dynamics both in space and time and may not report the full breadth of spatially heterogeneous dynamics in the system.

In addition to differences in probe size and probe–host interactions, differences in sample preparation could contribute to the differences seen in exchange time in the two SM studies in supercooled glycerol. Mackowiak *et al*. used a cooling rate of $\sim$5 K min$^{-1}$ while Zondervan *et al*. cooled approximately two orders of magnitude more slowly.[2,3] In the generally accepted view of the supercooled liquid as ergodic, cooling rate and time in the supercooled regime should not affect the behavior of the system so long as a crystalline transition is avoided. However, Xia *et al*. found patterns of micron length scale fluorophore density variations in supercooled glycerol, with the patterns differing with sample cooling rate.[6] A final factor that may have strongly influenced the different findings on temporal heterogeneity in the two SM experiments in glycerol relates to the manner in which temporal heterogeneity was assessed. The sliding window autocorrelation used by Mackowiak *et al*. reports on probe molecules, and presumably the surrounding host environments, that alter their dynamics from average to slower than average. This approach examines a portion of the "dynamic exchange phase space" between $\sim$10 and 300 $\tau_c$, or, for a rubrene probe, $\sim$100–3000 $\tau_\alpha$. On the other hand, the approach described in ref. 2 investigated changes over much longer time scales, and was directly sensitive to exchanges on time scales of $10^5$–$10^6$ $\tau_\alpha$. In this approach, molecules that do not exhibit exchange during the experiment can also be assumed not to have experienced exchange on time scales shorter than those probed directly (down to those time scales associated with accurate rate determination of rotational correlation times of the probe [$\sim$400 $\tau_\alpha$ for tbPDI]).

In this work, we use SM microscopy to monitor the rotations of three perylene probes, including the one used by Zondervan *et al*., in supercooled glycerol over the temperature range of 1.04–1.12$T_g$. This work aims to reconcile the findings of Mackowiak *et al*.[3] and Zondervan *et al*.,[2] investigate the temperature dependence of spatial and temporal heterogeneity as reported by perylene probes in glycerol, and more broadly investigate sensitivity of SM microscopy findings in supercooled liquids to probe size and interactions.

## II. Experimental

### A Sample preparation

Solid *N*,*N*′-bis(2,6-dimethylphenyl)-3,4,9,10-perylenedicarboximide (dpPDI), *N*,*N*′-bis[(3-dimethylamino)propyl]-3,4,9,10-perylenedicarboximide (dapPDI), and *N*,*N*′-bis(2,5-*tert*-butylphenyl)-3,4,9,10-perylenedicarboximide (tbPDI) are obtained from Sigma Aldrich (Fig. 2). dpPDI and tbPDI are provided as solids and are dissolved in ethanol (Sigma Aldrich, spectrophotometric grade) to obtain $\sim 1.0 \times 10^{-4}$ M concentration solutions. dapPDI is provided as a 1 mM solution in [2-*N*-morpholino]-ethanesulfonic acid and is diluted to $1 \times 10^{-6}$ M in ethanol. For dpPDI, 1.6 μL of $1.0 \times 10^{-7}$ M solution is added to 200 μL of glycerol giving a $8 \times 10^{-10}$ M dye concentration. For tbPDI, 2.0 μL of $1.0 \times 10^{-7}$ M is added to 100 μL of glycerol giving a $2 \times 10^{-9}$ M dye

View Online

Published on 26 November 2010 on http://pubs.rsc.org | doi:10.1039/C0CP01860K
Downloaded by Columbia University on 04 February 2011

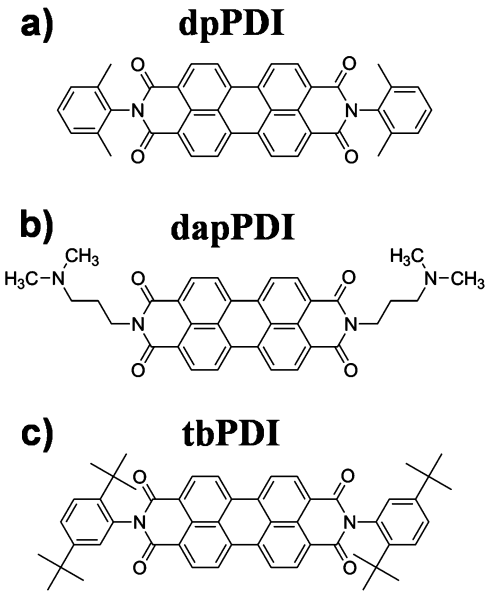


**Fig. 2** Perylene derivatives used in this study. (a) *N*,*N*′-bis-(2,6-dimethylphenyl)-3,4,9,10-perylenedicarboximide (dpPDI), molecular weight (MW) = 598.65 g mol$^{-1}$, (b) *N*,*N*′-bis[3-(dimethylamino)propyl]-3,4,9,10-perylenedicarboximide (dapPDI), MW = 560.64 g mol$^{-1}$, (c) *N*,*N*′-bis(2,5-*tert*-butylphenyl)-3,4,9,10-perylenedicarboximide (tbPDI), MW = 766.96 g mol$^{-1}$.

concentration. For dapPDI, a somewhat higher concentration is required for optimum number of visualized probe molecules per typical field of view. 2.0 μL of $1 \times 10^{-6}$ M dapPDI solution is added to 100 μL of glycerol to produce a $2 \times 10^{-8}$ M solution. The number of visualized molecules per typical field of view is comparable for all three probes, and the discrepancy in final concentration between the dapPDI and the other probes employed is assumed to be related to inaccuracy in the reported concentration of the purchased solution.

In all cases, the dye solutions are added to glycerol that is photobleached for 2 weeks in a bleaching setup.[11] To ensure mixing, the PDI/glycerol mixtures are heated for 20–60 min at 120 °C and shaken occasionally under exclusion of light to avoid photobleaching. The PDI/glycerol solutions are spin coat (Specialty Coating Systems, Model P6204) at 8000 rpm from a 120 °C solution onto a silicon wafer (University Wafer). Just prior to spin coating, each wafer is sonicated in acetone (Sigma Aldrich, spectrophotometric grade), rinsed with Millipore water, and heated briefly in an open flame to pyrolyze any remaining impurities and oxidize the surface to improve the wetting of the glycerol. The spin-coating procedure produces a glycerol film of several hundred nanometre thickness in the center of the wafer, as judged by the color of the film and the interference fringes.

The sample is placed into a microscopy cryostat (Janis Research Company Inc, Model ST-500-LN) using vacuum grease (Apiezon N) to optimize thermal contact between the sample stage and silicon wafer. The cryostat is evacuated and flushed with dry nitrogen five times at room temperature (at pressures no lower than 1 mTorr to prevent evaporation of glycerol) and subsequently cooled at ~5 K min$^{-1}$ to the desired temperature ($T$ = 198–212 K). Upon reaching the measurement temperature, the cryostat is evacuated for 1–2 h to a pressure of 0.3 mTorr. The evacuation procedure is required to remove water, which can be absorbed during spin coating. The water content of glycerol was confirmed to be reproducibly $<0.5\%$ both when removed from the bottle and after 15 min at atmospheric conditions by viscosity measurements. The time required for spin coating and transfer of the sample to the cryostat is ~5 min, after which the evacuation procedure is performed: we thus expect 0.5% water to be an upper bound on the water content.

### B Optical setup

Data are acquired using a home built microscope in an epi-fluorescence configuration as described in detail in ref. 3. The 514 nm line of an argon ion laser (Melles Griot 43 series, 543-APAO1) is the excitation source. The emitted light is directed through a laser line filter (Semrock, LL01-514), a $\lambda/2$ waveplate (Karl Lambrecht), and an electro-optic modulator (EOM; Conoptics, modulator M370 and amplifier 302RM). The waveplate aligns the polarization of the incoming laser light with the crystal axis of the EOM. The EOM switches the light between s and p polarization at a frequency of 1 kHz. A second $\lambda/2$ waveplate (Karl Lambrecht) after the EOM is used to align the incoming polarization to ensure a polarization ratio of at least 50 : 1 after the objective. The excitation beam is reflected towards the objective lens by a dichroic mirror (Semrock, FF520-Di01-25 × 36). The light is focused onto the rear focal plane of a long working distance objective with correction collar (Zeiss, LD Plan-Neofluar, air 63×, NA = 0.75, WD = 1.5 mm), resulting in a collimated excitation beam. This objective lens allows imaging through the 0.5 mm thick cryostat window with an additional separation of 0.25 mm between the cryostat window and sample. The illumination area is a circle of ~70 μm diameter. The fluorescence signal is collected by the objective in the epi-direction, passed through the dichroic mirror, and further filtered by a long pass filter (Semrock, LP02-514RS-25). Fluorescence is directed through a Wollaston prism (Karl Lambrecht) and another bandpass filter (Chroma, 600/150m) onto an EMCCD camera (Andor, iXon DV887). The Wollaston prism splits the signal into two orthogonal polarizations, resulting in two images on the CCD chip. 14-bit movies are recorded using LABView.

Data are collected at temperatures between 198–212 K. The frame rate is adjusted to ~20 frames per expected median rotational relaxation time of the probe, $\langle\tau_c\rangle$, as determined from preliminary experiments. For frame rates of 5–20 Hz (as are used for dpPDI at temperatures ≥ 208 K, dapPDI at temperatures ≥ 206 K, and tbPDI at temperatures ≥ 204 K), sample illumination is continuous, and exposure times are the inverse of the frame rate. The laser powers used for data collected at these frame rates are 6–24 mW, as measured before the objective. For frame rates of <5 Hz, sample illumination and exposure times are 0.2 s followed by a period without illumination of 0.3 s (2 Hz), 0.8 s (1 Hz), 1.3 s (0.67 Hz), 1.8 s (0.50 Hz), 2.8 s (0.33 Hz), 3.8 s (0.25 Hz), or 5.8 s (0.167 Hz). During the period without illumination, the

 This journal is © the Owner Societies 2011

View Online

Published on 26 November 2010 on http://pubs.rsc.org | doi:10.1039/C0CP01860K
Downloaded by Columbia University on 04 February 2011

**Table 1** Temperature, number of molecules, and FWHM for Gaussian ($FWHM_1$) and Lorentzian ($FWHM_2$) fits to the $\log(\tau_c)$ distributions shown in Fig. 4. FWHM are best-fits to within ±0.02

| | dpPDI | | | dapPDI | | | tbPDI | | |
|---|---|---|---|---|---|---|---|---|---|
| $T$/K | Molecules | $FWHM_1$ | $FWHM_2$ | Molecules | $FWHM_1$ | $FWHM_2$ | Molecules | $FWHM_1$ | $FWHM_2$ |
| 198 | — | — | — | 126 | 0.47 | 0.34 | 244 | 0.49 | 0.39 |
| 200 | 270 | 0.41 | 0.28 | 651 | 0.41 | 0.43 | 434 | 0.60 | 0.51 |
| 202 | 372 | 0.41 | 0.28 | 578 | 0.43 | 0.38 | 696 | 0.45 | 0.37 |
| 204 | 330 | 0.36 | 0.29 | 431 | 0.38 | 0.32 | 1319 | 0.79 | 0.67 |
| 206 | 438 | 0.38 | 0.29 | 748 | 0.41 | 0.37 | 1071 | 0.68 | 0.60 |
| 208 | 622 | 0.36 | 0.29 | 716 | 0.42 | 0.35 | 749 | 0.61 | 0.54 |
| 210 | 877 | 0.38 | 0.29 | 737 | 0.43 | 0.38 | — | — | — |
| 212 | 484 | 0.40 | 0.30 | — | — | — | — | — | — |
| **Average** | | **0.39** | **0.29** | | **0.42** | **0.37** | | **0.60** | **0.51** |

laser is shuttered with a mechanical shutter. Average powers used at these frame rates are 3–8 mW at 2 Hz, 1–4 mW at 1 Hz, 1–2 mW at 0.67 Hz, 1 mW at 0.5 Hz, 0.5–1 mW at 0.33 Hz, and 0.5 mW at 0.25 and 0.167 Hz. For a given sample at a given stage set temperature, data are collected at multiple laser powers to test and potentially correct for heating of the system, as described in the ESI.† The excitation powers and frame rates chosen yield data with similar signal to noise ratios across temperatures and allow collection of ~5000 frames per movie (at least 150 $\langle\tau_c\rangle$) with few molecules photobleaching early in the experiment. A total of 23, 29, and 51 movies are collected for dpPDI, dapPDI, and tbPDI, respectively. For dpPDI, all movies are collected on one sample over two days. For dapPDI and tbPDI, data are collected on two samples over three days each. The number of molecules analyzed at all temperatures for all probes is shown in Table 1.

### C Data analysis

As described in more detail in ref. 3, data analysis is performed using in house IDL based software (ITT Visual Information Solutions). The first 500 frames in a given movie are summed prior to identification of single molecules. The resulting summed movie image is filtered by convolution with a Gaussian intensity distribution. Individual features of a reasonable intensity above the background are then matched up into pairs—one from the left channel and one from the right channel—by using the known separation of the channels on the CCD chip. Only features that are identified in both channels and have characteristics consistent with single molecule fluorophores (reasonable intensity and single step bleach) are analyzed.

Once the locations of the fluorophores are established, all further analysis is performed on the raw, unfiltered images. The intensity of the fluorophore is calculated in both channels by integrating the intensities of pixels within 2–2.5 pixels of the identified feature center. In order to extract true fluorophore intensities, a spatially varying background that mimics the excitation beam profile is subtracted. The background is calculated for each molecule individually by averaging the intensities of the pixels surrounding the molecule from the limit of the intensity integration out to a radius of 4.5 pixels. In order to reduce the effect of other fluorophores that may border this background region, the top and bottom 10% of this distribution are excluded from the average. Background subtracted intensities are then recorded for each molecule in each frame of the movie. These intensities are denoted $I_{\parallel}$ and $I_{\perp}$. Linear dichroism (LD) is then constructed from each frame of the movies as

$$\mathrm{LD} = \frac{I_{\parallel} - I_{\perp}}{I_{\parallel} + I_{\perp}}. \quad (1)$$

LD values should span the range $-1 \leq \mathrm{LD} \leq 1$; however, due to inaccuracies in background estimation and subtraction, LD values outside the expected range are sometimes present. In order to exclude these unphysical values, when a negative intensity is present in one channel of the background subtracted signal, that value is set to zero. This procedure does not affect information subsequently obtained from the LD trajectory.[3]

The deviation of the LD signal from a mean, $a(t) = \mathrm{LD}(t) - \langle \mathrm{LD}(t) \rangle$, is used to construct an autocorrelation function (ACF):

$$C(t) = \frac{\sum_{t'} a(t')a(t'+t)}{\sum_{t'} a(t')a(t')}. \quad (2)$$

As detailed in ref. 3, while the ACF constructed from the SM LD signal is not an orientational correlation function of a single rank, given the experimental setup employed here, it is strongly dominated by $C_2(t)$, where $C_l(t) = e^{-Dl(l+1)t}$ with $D$ the rotational diffusion constant, and thus this experiment is a single molecule analogue to fluorescence anisotropy.[3,12,13] When the ACF is well fit by an exponential decay with time constant $\tau_{exp}$, that value can be taken as the rotational correlation time, $\tau_c$, of the probe. When the ACF is best fit by a stretched exponential decay given by

$$C(t) = A e^{-\left(\frac{t}{\tau_{fit}}\right)^{\beta}} \quad (3)$$

with $\beta$ the stretching exponent, the extracted relaxation time is given by

$$\tau_{str\ exp} = \frac{\tau_{fit}}{\beta} \Gamma\left(\frac{1}{\beta}\right). \quad (4)$$

Due in part to the limited length of the LD trajectories, better fits are generally obtained from the stretched exponential fits;[3,13,14] thus, all ACFs are first fit with the stretched exponential form. Because the goodness of fit for the stretched exponential varies with trajectory properties, trajectory dependent fitting is performed.[3] For molecules with low sampling rates (<20 points per $\tau_{str\ exp}$), $\tau_{str\ exp}$ is considered

View Online

Published on 26 November 2010 on http://pubs.rsc.org | doi:10.1039/C0CP01860K
Downloaded by Columbia University on 04 February 2011

the relaxation time, and $\tau_{str\ exp} = \tau_c$. For trajectories with high sampling rate and trajectories longer than 50 $\tau_{str\ exp}$, $\tau_{str\ exp}$ is also set as the relaxation time, $\tau_c$. For high sampling rate trajectories shorter than 50 $\tau_{str\ exp}$, a linear fit to the ACF is found to be more accurate than the stretched exponential fit.[3,15] Thus, these trajectories are re-fit to a line, ACF = $mt + b$ for the longer of either 20% of $\tau_{str\ exp}$ or five points. $\tau_c$ is then given by $b/m$.

### D Simulations

Criteria with which to assess the reliability and sensitivity of the two methods we use to detect molecules undergoing dynamic exchange are obtained using simulations of three dimensional *homogeneous* rotational diffusion of a fluorophore along the surface of a sphere. The transition dipole of a fluorophore is represented by a unit vector that is rotated, with the rotation axis chosen randomly for each step. The vector is rotated about this axis by an angle whose magnitude is chosen from a Rayleigh distribution, with the diffusion constant chosen to give the desired time constant, $\tau_c$. Simulations are performed at 20 points per $\tau_c$ for a trajectory length of 200 $\tau_c$, which approximates experimental conditions in this study.

From the simulated trajectories, *x*-, *y*-, and *z*-components of the dipole orientation are used to calculate intensity and linear dichroism as they would be detected experimentally. Specifically, $I_\parallel$ and $I_\perp$ are calculated assuming collimated excitation and epi-collection with an objective of NA = 0.75, as described in ref. 3. These intensities are scaled such that the average intensity correlates with that of a typical background subtracted experimental signal. Noise contributions are added to the simulated data. First, detector noise due to EM amplification of the CCD camera is considered. Detector noise has a variance ($\sigma^2$) two times the intensity of the signal,[16] and to add noise of this type to the simulations, each scaled intensity in the simulated trajectory is multiplied by a random number from a Gaussian distribution with mean equal to that intensity and variance equal to two times that intensity. Noise that may emerge from subtracting the spatially varying background is also included. Experimentally, after the probe fluorophore bleaches, the standard deviation of the (background subtracted) intensity fluctuations is at maximum 30% of the mean intensity of the signal before bleaching. Given that these fluctuations arise from several sources, 30% is considered an upper bound on the noise introduced by background subtraction. This additional "background noise" is added to the simulated signal. At every point in the simulated trajectory, a randomly chosen value from a Gaussian distribution centered at zero with standard deviation set to 30% of mean signal intensity (or $\sigma^2 = (0.3\ \mu_{signal})^2$) is added to the signal. After noise is added to the $I_\parallel$ and $I_\perp$ trajectories, as in the experimental traces, any negative intensities are set to zero. LD trajectories and ACFs are then calculated.

## III. Results and discussion

### A Median probe rotational relaxation times

In typical liquids, the temperature dependence of the host viscosity allows prediction of the rotational relaxation time of a probe of known size in the liquid *via* the Debye–Stokes–Einstein (DSE) equation,

$$\tau_c = \frac{V_h \eta(T)}{k_B T}. \quad (5)$$

The rotational relaxation time of the probeis given by $\tau_c$, $V_h$ is the hydrodynamic volume of the probe, $T$ is the temperature in Kelvin, $k_B$ is the Boltzmann constant, and $\eta(T)$ is the temperature dependent host viscosity. The DSE equation assumes a non-perturbative and spherical probe. Using the DSE equation to predict probe rotational relaxation time in a supercooled liquid also requires the assumption that DSE behavior holds in such systems. Experiments show that DSE behavior does describe probe rotations in small molecule supercooled liquids.[1,2,8,17] For the SM experiments described in this work, the rotational DSE equation is used primarily to confirm that measured SM probe dynamics are reflecting behavior of the host. We use the DSE equation both to compare the temperature dependence of the rotational relaxation of the probe to the known temperature dependent viscosity of glycerol and to extract a hydrodynamic volume, $V_h$, for the probe. Using the DSE equation allows us to confirm (1) collection of a statistically significant sample set, (2) that the temperature dependence of the probe's relaxation time tracks the viscosity of glycerol and thus reflects the host system's behavior on some level, and (3) a reasonable size for the probe.

Fig. 2 shows the structure and abbreviations for the three PDI probes used in this study: dpPDI, dapPDI, and tbPDI, the last of which was also used by Zondervan *et al.* for SM studies of supercooled glycerol.[2] The three molecules have similar photophysical properties, quantum yields near unity, and fluorescence anisotropy near the theoretical maximum of 0.4, making them well suited for SM measurement of rotational dynamics.[18,19] Median rotational relaxation times measured for each of the three probes as a function of temperature are plotted in Fig. 3. Each point represents the median $\tau_c$ from an individual movie (typically containing 100–200 analyzed probe molecules), which has been corrected for heating as described in the ESI.† The data are fit to the DSE equation using the known temperature dependence of the glycerol viscosity.[20] The determined hydrodynamic volumes of dpPDI, dapPDI, and tbPDI are $V_h = 2.02\ nm^3$ ($r_h = 0.79$ nm), $V_h = 1.27\ nm^3$ ($r_h = 0.67$ nm), and $V_h = 0.36\ nm^3$ ($r_h = 0.44$ nm), respectively.

The relative hydrodynamic volumes of the probes run counter to initial expectation, as it is generally accepted that a molecule with a larger space filling volume (which often trends with molecular weight) will rotate more slowly than a smaller and less massive molecule. Thus, tbPDI's rotations were expected to be slower and yield a larger hydrodynamic volume than dpPDI's due to the two *tert*-butyl groups in tbPDI compared to the two methyl groups in dpPDI. Instead, the measured hydrodynamic volume of dpPDI is ~5 times that of tbPDI, where our measurement is in close accord with the determined $V_h = 0.38\ nm^3$ obtained by Zondervan *et al.*[2] Similarly, the hydrodynamic volume of dpPDI is ~1.6 times greater than that of dapPDI despite the fact that these molecules' molecular weights differ by <10%. Indeed, the extracted probe hydrodynamic volumes are inconsistent with

 This journal is © the Owner Societies 2011

View Online

Published on 26 November 2010 on http://pubs.rsc.org | doi:10.1039/C0CP01860K
Downloaded by Columbia University on 04 February 2011

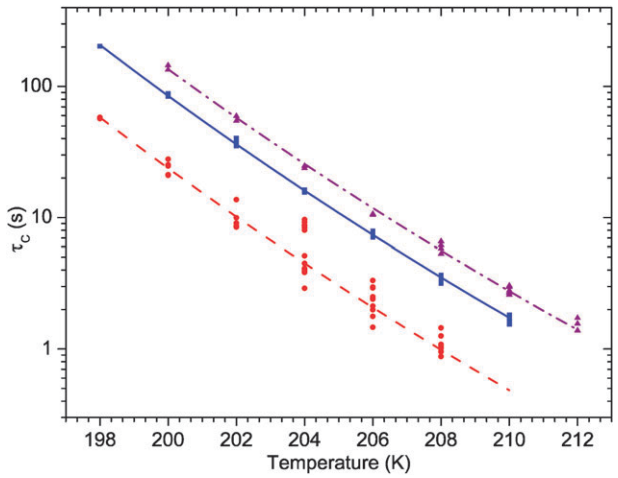


**Fig. 3** Rotational relaxation times *versus* temperature for tbPDI (red circles), dapPDI (blue squares), and dpPDI (purple triangles). Each point represents the heating corrected median $\tau_c$ for all molecules in a given movie. The lines are the fit of the DSE equation with best-fit hydrodynamic volumes for each of the probes. Red dashed line (tbPDI): $V_h$ = 0.36 nm$^3$, blue solid line (dapPDI): $V_h$ = 1.27 nm$^3$, and purple dash-dot line (dpPDI): $V_h$ = 2.02 nm$^3$.

an explanation based on probe mass or size such as that found by Wang and Richert for a variety of probe/host systems near $T_g$.[9] In that study, time resolved optical depolarization was used to monitor rotational relaxation of probe molecules while solvation experiments monitored solvent dynamics in the vicinity of the probes. It was found that the ratio of molecular weight of the probe relative to that of the host molecule, $R_m$, correlated with ratio of the rotational relaxation time of the probe to that of the host. Because our data are inconsistent with that finding, instead we consider the possibility that the measured hydrodynamic volumes reflect a complex mix of probe mass, space filling volume, structural anisotropy, and interactions with the surroundings.

Of the probes employed, dapPDI is expected to be the most polar and tbPDI the least polar.[18] Additionally, while all of these molecules may hydrogen bond with glycerol, in the case of tbPDI there may be steric hindrance that inhibits this interaction. Given the high polarity of glycerol and its hydrogen bonding network, differences in PDI probe polarity and ability to hydrogen bond are expected to affect probe interaction with the host, potentially slowing the rotation of hydrogen bonding probes relative to those that do not participate in the hydrogen bonding network. The suggestion that less polar molecules that cannot hydrogen bond with glycerol rotate more quickly than polar molecules of similar size that can participate in glycerol's hydrogen bonding network is also consistent with our previous result for rubrene in glycerol.[3] Rubrene has a similar mass to dapPDI and dpPDI but a significantly faster rotational relaxation time and thus a smaller extracted hydrodynamic volume ($V_h$ = 0.18 nm$^3$, data not shown) than any of the PDIs measured.[3] A similar slowdown for hydrogen bonding probes relative to non-hydrogen bonding probes has been noted previously in poly(isobutyl)methacrylate near $T_g$.[21] Given the slow rotation and large extracted $V_h$ for dapPDI and dpPDI, it is possible that these molecules' rotations are significantly hindered due to participation in the hydrogen bonding network or even that these probes are rotating with a shell or partial shell of glycerol molecules, increasing the effective radius of the probe.

### B Breadth of relaxation times

One of the chief reasons for evaluating the DSE behavior of the PDI dyes as a function of temperature is to establish the presence of a statistically significant sample size. Having found that all three probes exhibit changes in rotational relaxation time with decreasing temperature in accord with the DSE equation and known temperature dependence of the viscosity of glycerol, we now evaluate results that can only be attained from SM experiments. Fig. 4 shows the histograms of the heating corrected $\tau_c$ values for dpPDI, dapPDI, and tbPDI in the temperature range of 198 K–212 K. Qualitatively, the histograms for each of the PDI molecules look similar, and the histograms (on the log scale) are quite well fit by both Gaussian and Lorentzian functions. The Gaussian distribution is given by

$$y = \frac{1}{\sqrt{2\pi\sigma^2}} \exp^{-\frac{(x-x_c)^2}{2\sigma^2}}, \quad (6)$$

where $x_c$ indicates the center of the peak and $\sigma^2$ is the variance. The full width at half maximum (FWHM) is given by $2\sqrt{2\ln 2}\sigma$. The Lorentzian distribution is

$$y = \frac{1}{\pi} \times \frac{\gamma}{(x - x_c)^2 + \gamma^2} \quad (7)$$

with the FWHM given by $2\gamma$. Taking the adjusted $R^2$ value as an indicator of the quality of the fit, both distributions fit the histograms equally well. In Table 1, the number of assessed molecules and the FWHM from the Gaussian and Lorentzian fits are shown for each probe at each temperature investigated, and Fig. 4 shows Gaussian fits to the distributions of $\tau_c$ values for dpPDI, dapPDI, and tbPDI for all single molecule probes evaluated in this study. While these distributions are well fit by symmetric functions on a log scale, on a linear scale the data are well described by log-normal distributions, which have previously been associated with non-trivial, cooperative dynamics.[22]

The distributions shown in Fig. 4 indicate that there is a spread of rotational relaxation times reported by all of the probes in supercooled glycerol at all of the temperatures investigated, with molecules exhibiting rotational relaxation times that span at least an order of magnitude at all temperatures and for all probes studied. This implies that dpPDI, dapPDI, and tbPDI all report spatial heterogeneity in supercooled glycerol. While the log-normal distributions evident here represent a large spread of time constants, the histograms are significantly different in shape from that of rubrene in glycerol at 204 K, which had a more prominent long time tail and a spread of time constants that spanned nearly three orders of magnitude.[3] This suggests that rubrene accesses and reports a larger breadth of the environments in supercooled glycerol than do the larger, more slowly rotating PDI probes. It is also evident that the distributions of time scales reported by the SM probes are narrower and somewhat

View Online

Published on 26 November 2010 on http://pubs.rsc.org | doi:10.1039/C0CP01860K
Downloaded by Columbia University on 04 February 2011

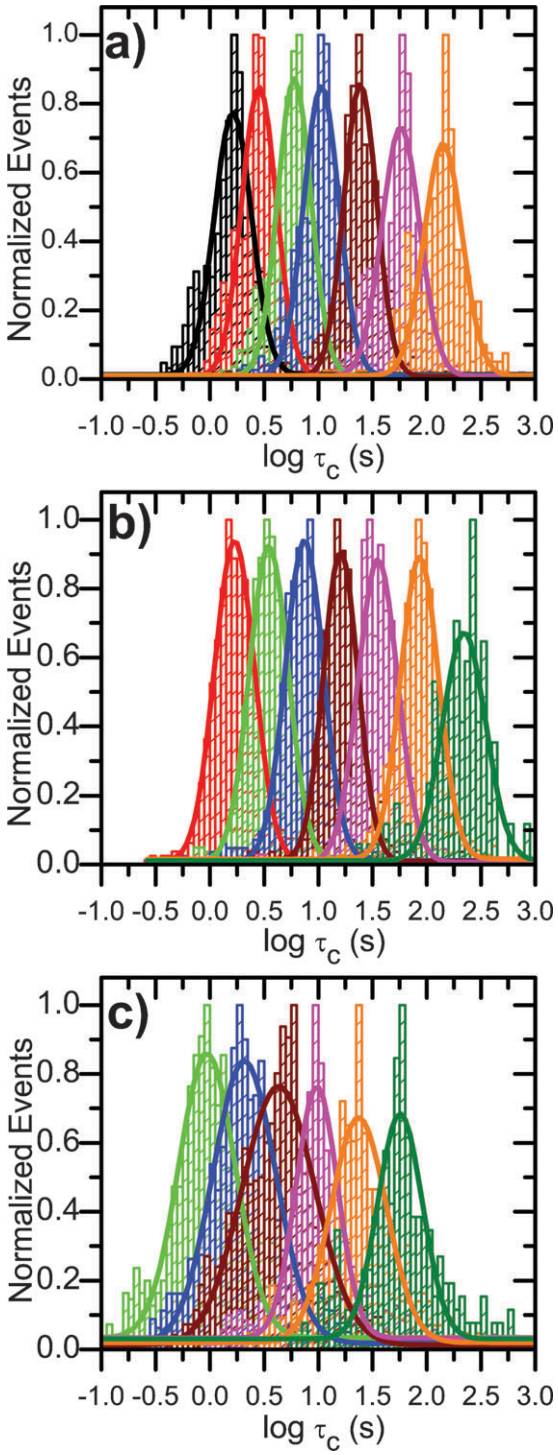


**Fig. 4** Histograms of log($\tau_c$) values for all PDI probes with Gaussian fits: (a) dpPDI, (b) dapPDI, and (c) tbPDI. Colors indicate temperature: black: 212 K, red: 210 K, green: 208 K, blue: 206 K, wine: 204 K, magenta: 202 K, orange: 200 K, forest green: 198 K. All histograms are normalized to the maximum number of occurrences at each temperature. Because dapPDI and tbPDI are taken from two data sets, to make this data comparable to that of dpPDI, collected on one sample, a normalization is performed. Two histograms are made (one for each of the data sets collected) for dapPDI and tbPDI and each histogram is normalized such that median $\tau_c$ at a given temperature matches that from the best-fit DSE fit. This prevents histogram width from being affected by potential differences between data sets.

different in shape than would be expected from results of a variety of bulk measurements in supercooled glycerol.[20,23]

Given that all measured histograms are well fit with Gaussians and Lorentzians, differences in histogram shape as a function of temperature and probe can be assessed straightforwardly through the FWHM of the best-fit curve to the distributions. Turning first to histogram shape as a function of temperature, no clear trends are observed. For example, for dpPDI, distributions at all temperatures are best fit by Gaussian functions with FWHM between 0.36 and 0.41 (±0.02) or Lorentzians with FWHM between 0.28 and 0.30 (±0.02). The finding of a constant histogram width as a function of temperature is consistent with the principle of time temperature superposition (TTS). The TTS principle states that the imaginary part of the response function of a dynamic property, such as viscosity or α-relaxation time probed as a function of frequency, has the same shape at different temperatures.[24] Thus, a response curve at one temperature can be overlapped with a response curve at a different temperature by shifting the frequency axis. This ability to collapse all response curves onto a master curve suggests that the dynamics governing supercooled behavior remain similar in some regards over the temperature range between $T_m$ and $T_g$. For molecular glass formers, TTS has often been found to hold in the low frequency regime, which is equivalent to the long time relaxations monitored here, but not at high frequency.[24] When one considers spatially heterogeneous dynamics, it is not obvious that the extent of heterogeneity should be the same over the full supercooled temperature regime. It may then be expected that observables that probe these heterogeneities directly may vary with temperature even if TTS holds when probing bulk observables. Despite this, for PDI probes, the shape and width of histograms detailing spatial heterogeneity *via* SM microscopy are found to be constant as a function of temperature in supercooled glycerol in the range of 1.04–1.12 $T_g$.

The fact that the distributions of rotational relaxation times measured are not changing shape with temperature suggests that degree of spatially heterogeneous dynamics in glycerol is constant over the temperature range probed. However, comparing the widths of the distributions at each temperature across PDI probes reveals the dapPDI $\tau_c$ distributions to be slightly wider than those of dpPDI at all temperatures. A more notable difference is apparent between the $\tau_c$ distributions for tbPDI and those for dpPDI and dapPDI. Data collected using tbPDI are more variable than for either of the other two probes, with the histograms for relaxation times at some temperatures slightly broader than those for dapPDI and at some temperatures significantly broader, though with no clear trend as a function of temperature. The breadth of the tbPDI histograms is confirmed not just for the pooled data over the two samples and 53 movies represented in Fig. 4 but also for the 100–200 molecules in individual movies, showing that the increased breadth of rotational relaxation times in the tbPDI data is not due to movie to movie or sample to sample variation in median relaxation time that can be seen in the spread of points for tbPDI at a given temperature in Fig. 3.

Given the similar size of the three PDI probes used in this work and the fact that tbPDI is the largest of these probes, we

 This journal is © the Owner Societies 2011

View Online

Published on 26 November 2010 on http://pubs.rsc.org | doi:10.1039/C0CP01860K
Downloaded by Columbia University on 04 February 2011

suggest that the narrower $\tau_c$ distributions seen for the dpPDI and dapPDI relative to those of tbPDI are unlikely to be due to a differential in spatial averaging by the probes. Instead, the broad distribution found for tbPDI suggests that more quickly rotating probes can report the presence of a more significant breadth of spatially heterogeneous dynamics in the glycerol host and that the narrowing of dpPDI and dapPDI histograms relative to those seen for tbPDI is driven by the increased temporal averaging of the more slowly rotating dpPDI and dapPDI probes. This is also supported by comparing $\tau_c$ distributions for two probes in glycerol at different temperatures chosen such that the median probe $\tau_c$ overlaps. In Fig. 5, the $\tau_c$ distributions for tbPDI at 200 K and dpPDI at 204 K are shown: both distributions peak at $\sim$20 s, but the tbPDI distribution is broader. In this comparison, the time averaging in absolute time performed by the probes over the spatially heterogeneous dynamics is the same for most probe molecules in the glycerol. Given the similarity in the probe molecular structure, the spatial averaging is also expected to be very similar, with tbPDI averaging slightly more than dpPDI in space owing to its *tert*-butyl groups. Comparing these two distributions from probes that have performed very similar temporal and spatial averaging over their surroundings may suggest that glycerol at 200 K is more heterogeneous than glycerol at 204 K, as judged from the breadth of the distributions at the two temperatures. However, taken in the context of Fig. 4, in which we find no broadening with decreased temperature for a given probe, we suggest that this behavior is further evidence for temporal averaging by the probes being the primary determinant of the breadth of $\tau_c$ distribution: even while the absolute time averaging between the two probes is the same in the two distributions shown in Fig. 5, the relative $\tau_c/\tau_\alpha$ values are $\sim$16 for tbPDI at 200 K and 90 for dpPDI at 204 K. As such, the effective time averaging relative to the structural relaxation time of the surroundings is greater for the dpPDI probe at the higher temperature, consistent with the narrower distribution found. Such temporal averaging has been implicated previously in probe molecules' inability to report the full breadth of heterogeneity in a supercooled liquid in ensemble and sub-ensemble measurements.[10] This conclusion is also consistent with results for rubrene probes in glycerol at 204 K, which show a distribution of probe rotational relaxation times that has a long time tail and a distribution spanning nearly three orders of magnitude.[3]

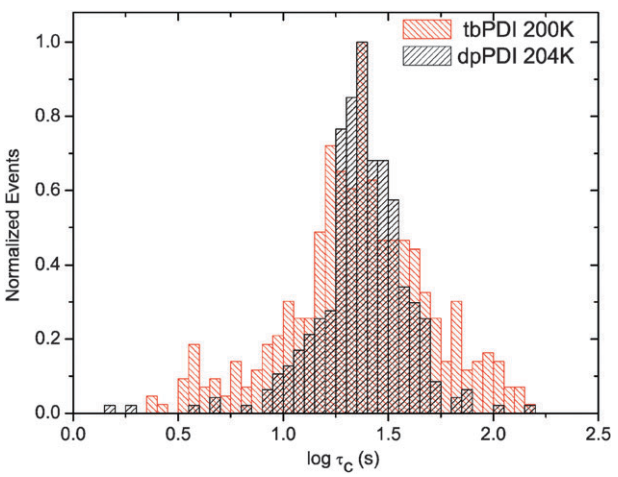


**Fig. 5** Histograms of log($\tau_c$) values for dpPDI at 204 K and tbPDI at 200 K. The two distributions are centered at approximately the same value, and absolute temporal and spatial averaging performed by the probes are expected to be very similar.

The conclusion that time averaging is responsible for the differential in rotational relaxation time distribution breadth between the probes suggests that dynamic exchange occurs on time scales shorter than or similar to probe rotation. While other measurements have also led to the finding that large probes will average over spatially heterogeneous dynamics in space and/or time, as depicted in Fig. 1, we note here that we find strong evidence for spatially heterogeneous dynamics in supercooled glycerol in these SM experiments for probes that are quite large. While other studies report that probes of molecular weight $\geq$ 1.2 times that of the host and/or relaxation times $\geq$ 20 times the solvent relaxation time exhibit exponential decays in optical depolarization experiments,[9] implying full averaging over the spatially heterogeneous dynamics in the sample, in these experiments we find a broad spread of spatially heterogeneous dynamics even for tbPDI, whose molecular weight is 8.3 times that of the host molecule. This behavior is further investigated by considering the average ACF as would be measured *via* bulk experiments. Averaging the LD ACFs for 629 tbPDI molecules at 204 K and fitting the resulting ACF to a stretched exponential yields a best-fit stretching exponent of 0.88. This is the first time a molecule as large as tbPDI ($\sim$8 times the molecular weight of and $\sim$20 times slower than glycerol) has demonstrated deviations of the stretching exponent from unity. These findings confirm that in supercooled glycerol even the relatively large and slow probes used in SM studies to date are sensitive to spatially heterogeneous dynamics in supercooled glycerol.

### C Dynamic exchange

The broader spread of rotational relaxation times seen for probe molecules that, on average, rotate most quickly despite similar molecular weight and structure suggests the presence of dynamic exchange on time scales on or shorter than that associated with probe rotation ($\sim$100 $\tau_\alpha$ for dpPDI and 20 $\tau_\alpha$ for tbPDI). To more directly assess temporal heterogeneity and dynamic exchange, two techniques that directly interrogate dynamic exchange on time scales from $10^3$–$10^6$ $\tau_\alpha$ are employed.

**1 Window shifting technique.** A method proposed by Schob *et al.* is employed to detect changes in dynamics during the collected trajectories.[25] The LD trajectory is split up into segments by a window that is slid across the trajectory, and an ACF is calculated and fit for each segment. This results in a trajectory of rotational time constants, subsequently called $\tau$-trajectory. A sliding window of 20 $\tau_c$, with $\tau_c$ the rotational relaxation time obtained from the full trajectory, is selected to balance sensitivity to relatively short changes in dynamics and accuracy and precision of ACF fits. The window is moved by 10 points ($\sim$0.5 $\tau_c$) between each fitted window. Linear fitting is used to derive $\tau_c$ in each window due to the short window

View Online

Published on 26 November 2010 on http://pubs.rsc.org | doi:10.1039/C0CP01860K
Downloaded by Columbia University on 04 February 2011

width and insensitivity of linear fits to window width.[3] After $\tau$-trajectory is obtained, a molecule is classified as either temporally heterogeneous or homogenous using criteria set with simulations described in the Experimental section.

For simulations of homogeneous rotational diffusion, 95% of the trajectories are found to have 95% of their $\tau$-trajectory values within 2.6 times the median relaxation time in $\tau$-trajectory ($\tau_{traj,med}$). This criterion thus has a false positive rate of 5%. A second criterion is based on the finding that 95% of the homogeneous trajectories have $\tau$-trajectory distributions with standard deviations $<0.68$. The second criterion is thus satisfied if the standard deviation of $\tau$-trajectory is $>0.68$. These criteria were developed for trajectories of 200 $\tau_c$ with a point density of 20 points per $\tau_c$, properties chosen to well match the experimental data. Molecules are assigned as heterogeneous if either the first or second criterion is met. Using these criteria, between 5 and 10% of homogeneous molecules are expected to be incorrectly identified as heterogeneous.

This approach has been applied to data collected on dpPDI at all temperatures as well as for dapPDI and tbPDI at 204 K. For dpPDI, all molecules in all movies are investigated for potential temporal heterogeneity *via* this approach. For dapPDI and tbPDI, at least two movies each collected at 204 K are assessed. In all cases, the total number of molecules in the movies are only assessed for temporal heterogeneity with the sliding window technique when the LD trajectory is $>50$ $\tau_c$ and $\tau$-trajectory contains both at least 50 points and at least 33% of the expected points based on window step, window size and trajectory length. Missing points in $\tau$-trajectory are usually due to a noisy ACF obtained from a particular window. This typically manifests as a poor fit to the ACF, with $\tau_c$ from a linear fit and an exponential fit differing by more than a factor of 3 or a pre-exponential factor lower than 0.3, either of which results in the point being excluded from $\tau$-trajectory. With these criteria, $\sim$75% of molecules that are present in each movie are assessed for temporal heterogeneity with the window shifting approach. As can be seen in Table 2, 26–36% of dpPDI molecules assessed are found to be heterogeneous by this approach, with no clear dependence on temperature. At 204 K, dapPDI shows similar results, with $\sim$25% of molecules found to be heterogeneous; however, for tbPDI at 204 K only 15% of the assessed molecules satisfy the criteria for heterogeneity. Taken together with previous work showing 15% of rubrene molecules in supercooled glycerol at 204 K were classified as heterogeneous with this approach,[3] the tbPDI data suggest that faster probes may be less likely to be classified as heterogeneous in the sliding window approach. This may be related to the fact that dpPDI and dapPDI show a relatively narrow distribution of $\tau_c$ values relative to rubrene and tbPDI. Thus, the dynamic exchanges likely to occur for dpPDI and dapPDI (alterations in time constant of a factor of $\sim$2–3) may be more readily picked up by the window shifting technique than are those that rubrene and tbPDI undergo. Indeed, unlike in the rubrene data, no evidence of molecules exchanging between dynamically disparate environments is present for dpPDI or dapPDI though a small proportion of tbPDI molecules do exhibit large, abrupt changes in dynamics (data not shown) as were also seen for rubrene.[3]

**Table 2** Number of molecules assessed for heterogeneity and found to be heterogeneous with the sliding window approach

| $T$/K | Assessed molecules | Heterogeneous molecules | Percent heterogeneous |
|---|---|---|---|
| | dpPDI | | |
| 200 | 166 | 59 | 35.5 |
| 202 | 226 | 80 | 35.4 |
| 204 | 243 | 70 | 28.8 |
| 206 | 319 | 84 | 26.3 |
| 208 | 307 | 80 | 26.1 |
| 210 | 606 | 166 | 27.4 |
| 212 | 321 | 114 | 35.5 |
| | dapPDI | | |
| 204 | 220 | 54 | 24.5 |
| | tbPDI | | |
| 204 | 194 | 29 | 15.0 |

For dpPDI at all temperatures as well as for dapPDI and tbPDI at 204 K, for each molecule assigned as heterogeneous, $\tau$-trajectory is evaluated for time until the first change in dynamics and, potentially, for time between dynamic exchanges. The time before the first change in dynamics is termed the persistence time ($\tau_{pers}$) and that between changes in dynamics is the exchange time ($\tau_{ex}$), in keeping with definitions employed for kinetically constrained models.[26] The values and temperature dependence of persistence and exchange time need not be the same, and thus we distinguish between them. Lower bounds on exchange times (time from last exchange of a heterogeneous molecule to the end of the evaluated portion of the LD trajectory) as well as lower bound on persistence time (time to the end of the evaluated portion of the LD trajectory for homogeneous molecules) are also tabulated. Histograms of the ratios of exchange, lower bound on exchange, persistence, and lower bound on persistence time to the molecules' rotational relaxation times for the 70 heterogeneous molecules identified in dpPDI at 204 K are shown in Fig. 6. The median ratio of the molecules' lower bound on persistence times relative to their rotational correlation times ($\tau_{pers,lower\ bound}/\tau_c = 145$) is significantly longer than that of persistence times relative to rotational correlation times measured on molecules that experience exchange ($\tau_{pers}/\tau_c = 26$). This is similar to the findings in rubrene at 204 K and consistent with the idea that a molecule undergoing exchange is likely to continue to do so. Exchange and lower bound on exchange times relative to rotational relaxation time from molecules deemed heterogeneous are found to be $\tau_{ex}/\tau_c = 36$ and $\tau_{ex,lower\ bound}/\tau_c = 43$. Examining these quantities as a function of temperature reveals they are relatively insensitive to temperature (Fig. 7). Only the lower bound on persistence time exhibits a clear trend with respect to temperature, increasing monotonically with temperature from $\tau_{pers,lower\ bound}/\tau_c \approx 110$ at 200 K to $\approx$170 at 210 and 212 K. However, this trend appears correlated with the total median trajectory lengths of the assessed molecules. Indeed, the trajectory lengths of not only the molecules classified as homogeneous but also those classified as heterogeneous follow this trend. This is displayed in a quantity termed

 This journal is © the Owner Societies 2011

View Online

Published on 26 November 2010 on http://pubs.rsc.org | doi:10.1039/C0CP01860K
Downloaded by Columbia University on 04 February 2011

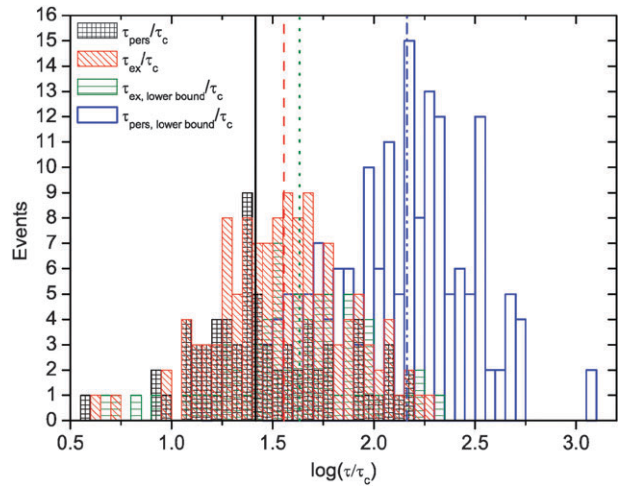


**Fig. 6** Histograms and median values (lines) of $\tau_{pers}/\tau_c$ (black bars with checks; black solid line), $\tau_{ex}/\tau_c$ (red bars with diagonal lines; red dashed line), $\tau_{ex,lower\ bound}/\tau_c$ (olive bars with horizontal lines; olive dotted line), and $\tau_{pers,lower\ bound}/\tau_c$ (blue bars; blue dash-dot line) as compiled from the 243 dpPDI molecules assessed for temporal heterogeneity at 204 K.

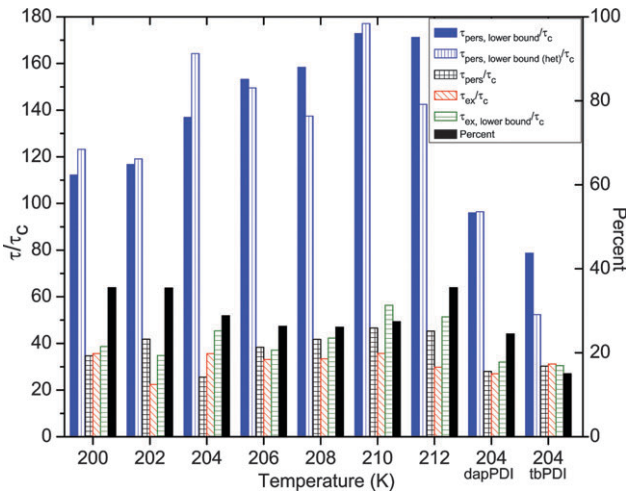


**Fig. 7** Median $\tau_{pers}/\tau_c$ (black bars with checks), $\tau_{ex}/\tau_c$ (red bars with diagonal lines), $\tau_{ex,lower\ bound}/\tau_c$ (olive bars with horizontal lines), $\tau_{pers,lower\ bound}/\tau_c$ (blue bars), and $\tau_{pers,lower\ bound\ (het)}/\tau_c$ (blue bars with vertical lines) as a function of temperature for dpPDI as well as for dapPDI and tbPDI at 204 K.

$\tau_{pers,lower\ bound(het)}/\tau_c$ in Fig. 7. For dapPDI (tbPDI) at 204 K, the median values are $\tau_{pers,lower\ bound}/\tau_c = 96$ (79), $\tau_{pers}/\tau_c = 28$ (30), $\tau_{ex}/\tau_c = 27$ (31) and $\tau_{ex,\ lower\ bound}/\tau_c = 32$ (31), with similar distributions for each of these quantities as those shown for dpPDI in Fig. 6 (data not shown).

The various time scales shown in Fig. 7 can be translated into values relative to $\tau_\alpha$ using the ratio $\tau_c/\tau_\alpha$ for each of the probes. This ratio varies between $\sim$100 for dpPDI and $\sim$20 for tbPDI. As such, $\tau_{ex}/\tau_\alpha \approx 3600$ for dpPDI and $\tau_{ex}/\tau_\alpha \approx 600$ for tbPDI (and was $\approx$200 for rubrene) in glycerol at 204 K. Given the similarity in $\tau_{ex}/\tau_c$ values for the various probes, the large spread in $\tau_{ex}/\tau_\alpha$ values highlights how probe speed sensitively influences time scale on which dynamic exchange can be assessed. Despite the fact that for all probes at all temperatures the window shifting technique is sensitive to exchange on the order of $\sim$10–200 $\tau_c$, this translates into different sensitivities in the "dynamic exchange phase space" relative to $\tau_\alpha$. As will be described further below, the insensitivity of $\tau_{ex}/\tau_c$ and related values to temperature and probe also suggests that the window shifting technique is reporting a bound on average exchange time rather than an absolute value of this quantity.

**2 Long time heterogeneity assessment.** To supplement analysis of temporal heterogeneity and dynamic exchange provided by the window shifting technique, a variation on the long time heterogeneity assessment carried out by Zondervan *et al.* is performed.[2] This technique can directly probe dynamic exchange on time scales longer than those assessed by the window shifting technique. It can thus address whether molecules appear homogeneous by that method ($\sim$65–85% of the assessed molecules) do so because exchange occurs on time scales longer than those associated with typical trajectory length. To perform this experiment, several movies of the same dpPDI probe molecules embedded in glycerol at 210 K are collected consecutively. Specifically, we collect a movie of trajectory length $\sim$ 50 $\langle\tau_c\rangle$, wait $\sim 10^5\ \tau_\alpha$, collect a second $\sim$50 $\langle\tau_c\rangle$ movie of the same molecules, wait $\sim 10^6\ \tau_\alpha$, and collect a third $\sim$50 $\langle\tau_c\rangle$ movie of the same molecules. In one case, the trajectories collected are $\sim$75 $\langle\tau_c\rangle$ and only two movies are collected, with a waiting time of $\sim 10^6\ \tau_\alpha$. The relatively short trajectories are required to prevent photobleaching of the molecules before the experiment is complete. However, we focus on maximizing trajectory length within this constraint, given that the accuracy of extracted rotational correlation times from the ACFs depends strongly on trajectory length for short trajectories.[3,14] This experiment allows comparison of SM relaxation times after fixed waiting times very long compared to $\tau_\alpha$ and, as such, provides sensitivity to temporal heterogeneity that may occur on time scales much longer than that provided by the window shifting technique, whose long time sensitivity limit is similar to typical trajectory length ($\sim 200\ \tau_c \approx 10^3$–$10^5\ \tau_\alpha$, depending on probe). In the long time heterogeneity experiment, a molecule experiencing dynamic exchange on any time scale faster than the waiting times is expected to have different relaxation times in each of the movies.

As with the window shifting approach, simulations are performed on molecules undergoing homogeneous rotational diffusion to set criteria for heterogeneity and to assess the accuracy and sensitivity of the method. This is especially important given that ACFs constructed from trajectories between 10–250 $\tau_c$ have intrinsic uncertainty, and even molecules undergoing homogeneous rotational diffusion with unchanging relaxation dynamics may appear to have different time constants over time as a result of this uncertainty.[14] Homogeneous rotational diffusion of 1000 molecules is simulated. The population is set to have a $\tau_c$ distribution with a FWHM of 0.4 on a log-scale, $\langle\tau_c\rangle$ of 20 steps, and a trajectory length of 1000 steps ($50\langle\tau_c\rangle$), similar to data collected on dpPDI. As described in the Data analysis section, trajectory dependent fitting of the LD ACFs is

View Online

Published on 26 November 2010 on http://pubs.rsc.org | doi:10.1039/C0CP01860K
Downloaded by Columbia University on 04 February 2011

performed. The $\tau_c$ value for each molecule is normalized to its minimum value over the 2–3 movies (or simulated data sets), and the 2–3 $\tau_c$ values are plotted for each molecule relative to this minimum. Normalizing $\tau_c$ to the minimum value facilitates assessment of temporal heterogeneity by removing the effect of the relatively broad spread of time constants in the simulated or experimental data.

For 3 (2) simulated trajectories of 50 $\langle\tau_c\rangle$, 95% of the molecules are found to have a maximum $\tau_c$ value within 3.0 (2.7) times the minimum $\tau_c$ value of that molecule, and 90% have a maximum value within 2.7 (2.2) times the minimum $\tau_c$ value of that molecule. Because one of our experiments of this type was performed with 2 trajectories of 75 $\langle\tau_c\rangle$, simulations for 2 trajectories of that length are also performed. Here, the 95% confidence interval (CI) is 2.1 and the 90% CI is 1.9. Concentrating on the result for 3 consecutive 50 $\langle\tau_c\rangle$ trajectories, we conclude that due to statistical variation, a molecule with homogeneous dynamics can have a change of $\tau_c$ by a factor of 3 as assessed by experiments of this type. This is a greater variation in $\tau_c$ than is expected for homogeneous rotational diffusion as examined with the window shifting approach. This is due to the fact that there the assessed trajectories are known to be 20 $\tau_c$ in all cases, while in this experiment and simulation the trajectories are 50 $\langle\tau_c\rangle$, or on average 50 $\tau_c$. Slower than average molecules have trajectories shorter than 50 $\tau_c$, leading to substantial uncertainty in the time constants extracted for these molecules. Moreover, in the window shifting approach, the change in $\tau_c$ is relative to $\tau_{traj,med}$, where here it is relative to a value that is likely to be smaller, the minimum $\tau_c$ in the 3 windows. For three trajectories of 50 $\langle\tau_c\rangle$, given that simulations reveal that 95% of molecules will have a maximum $\tau_c$ value within 3.0 times the minimum $\tau_c$ value, we conclude that if more than 5% of the molecules have a change in $\tau_c$ greater than a factor of 3.0, temporal heterogeneity is observed. Fig. 8a shows the simulation results for 3 trajectories of 50 $\langle\tau_c\rangle$ length for 100 randomly chosen simulated molecules. It is evident that there is substantial crossing of the lines tracking the rotational relaxation times of particular particles. This may initially look to suggest temporal heterogeneity, but we stress that this simulation is for homogeneous rotational diffusion, and all changes in dynamics are due solely to statistical uncertainties.

Given that for the 50 $\langle\tau_c\rangle$ window experiments the lower limit of sensitivity is a change of $\tau_c$ of a factor of 3, we consider how likely it is that this experiment will show clear evidence for temporal heterogeneity in the data evaluated. The distribution of $\log(\tau_c)$ values was modeled to be Gaussian with a FWHM of 0.4, consistent with data collected using dpPDI and dapPDI. For such a distribution, the standard deviation, $\sigma$, is 0.17. Thus, if this distribution is centered at 20 steps ($\log(20) = 1.3$), ~67% of the molecules are expected to have $\tau_c$ values between 13.5 steps ($\log(13.5) = 1.13$) and 29.5 steps ($\log(29.5) = 1.47$). 90% (1.64 $\sigma$) of the molecules will have a relaxation time $\tau_c$ between 10.5 steps and 38.0 steps. Assuming that molecules undergoing dynamic exchange experience no bias in that exchange (*i.e.*, a molecule in the fastest decile of molecules is as likely to become a molecule in the slowest decile as any other possible exchange), it is expected that even if all molecules exhibit exchange during the full time course of the experiment, only ~10% of the molecules will experience changes of $\tau_c$ of a factor of 3 or more.[27] Considering the 95% confidence interval described above, these findings require discrimination of this 10% from the 5% of molecules that may experience this substantial of a change even without any change in dynamics. Thus, our initial expectation is that this method will give a null result, neither proving nor excluding the possibility that temporal heterogeneity and dynamic exchange are present. To assess a data set for the presence of temporal heterogeneity *via* the method described here would require a very large number of molecules such that the rare relatively large changes in dynamics possible would be seen in sufficient numbers to discriminate them from those that may occur from statistical variation alone. However, because this approach is similar to the approach used by Zondervan *et al.*, and because it does allow probing exchanges on time

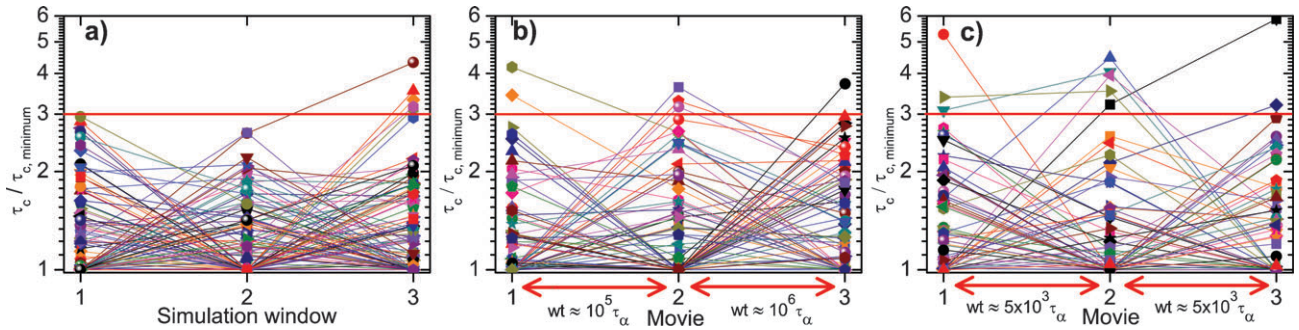


**Fig. 8** Long time heterogeneity assessment for (a) simulations and (b, c) experiments. Points connected by lines across the three simulated or experimental windows represent individual simulated or experimental molecule. In all cases, the $\tau_c$ values are normalized by the minimum $\tau_c$ value for each molecule. The red lines indicate the 95% confidence interval (CI) from simulations as described in the text. In panels (b) and (c), "wt" is waiting time. (a) $\tau_c$ values for 3 simulated 50 $\langle\tau_c\rangle$ trajectories. Of the 1000 simulated trajectories, 100 are chosen at random for display. (b) Molecules from one of two experiments in which 3 movies of trajectory length 50 $\langle\tau_c\rangle$ separated by $10^5$ $\tau_\alpha$ and $10^6$ $\tau_\alpha$, respectively, were collected. Only molecules that have well fit ACFs for all 3 movies are included. In this movie, 6 of 64 (9.4%) molecules are above the 95% CI. (c) Molecules from one movie of dpPDI at 210 K collected for ~200 $\langle\tau_c\rangle$, yielding 4 windows of 50 $\langle\tau_c\rangle$. All molecules with three consecutive windows of 50 $\langle\tau_c\rangle$ with LD ACFs that are well fit are included. In this movie, 7 of 58 (12.0%) molecules are above the 95% CI. For the five movies analyzed, 57 of 431 molecules are above the 95% CI (13.2%).

 This journal is © the Owner Societies 2011

View Online

Published on 26 November 2010 on http://pubs.rsc.org | doi:10.1039/C0CP01860K
Downloaded by Columbia University on 04 February 2011

scales significantly longer than does the window shifting technique, we describe results from this approach on dpPDI at 210 K. The relatively high temperature ($1.11T_g$) is employed so that multiple movies separated by $10^5$–$10^6$ $\tau_\alpha$ can be collected within several hours, thus avoiding potential issues with mechanical stability.

Fig. 8b displays results from such experiments on dpPDI in glycerol at 210 K. In the experiment represented by Fig. 8b, the first two movies are separated by $\sim 10^5$ $\tau_\alpha$ and the second and third movies are separated by $\sim 10^6$ $\tau_\alpha$. While changes in extracted $\tau_c$ are clearly occurring, as evidenced by the many lines that cross each other in Fig. 8b, most of the measured $\tau_c$ values fall below the 95% CI denoted by the red line at 3.0. Indeed, comparing Fig. 8a and b reveals no qualitative differences despite the fact that Fig. 8a is based only on homogeneous dynamics. However, subtle differences are noted when evaluating the data shown in Fig. 8b as well as related experiments. Specifically, 6 of 64 molecules (9.4%) followed for 3 movies of 50 $\langle\tau_c\rangle$ (Fig. 8b) and 6 of 62 molecules (9.7%) followed for 2 movies of $75\langle\tau_c\rangle$ (not shown) fall outside the 95% CI as set by simulations of molecules undergoing homogeneous rotational diffusion. In both cases, $\sim$10% of the molecules appear to change their dynamics, double the proportion that would be expected given homogeneous rotational diffusion. As described above, for the breadth of spatial heterogeneity observed for dpPDI, this result is consistent with the presence of temporal heterogeneity and unbiased dynamic exchange. However, the total number of molecules investigated is relatively small (126 molecules). Thus, while this experiment may be evidence of probe molecules exhibiting dynamic exchange, observing a larger number of molecules would be necessary to confirm this finding.

Performing analysis on the molecules represented in Fig. 8b not on molecules that have LD trajectories well fit by ACFs in all three of the movies, but on molecules that have LD trajectories well fit by ACFs in either the first two movies (with a waiting time of $\sim 10^5$ $\tau_\alpha$) or the second two movies (with a waiting time of $\sim 10^6$ $\tau_\alpha$) allows assessment of whether there is more exchange occurring on the longest time scales probed (between $10^5$ and $10^6$ $\tau_\alpha$) than at all times shorter than $10^5$ $\tau_\alpha$. If substantial exchange is occurring on these longest time scales, a higher proportion of molecules should fall outside the 95% CI as waiting time increases. It is found that 9 of 121 molecules and 11 of 123 molecules fall outside the 95% CI (2.7 for 2 movies of 50 $\langle\tau_c\rangle$) for waiting times of $\sim 10^5$ $\tau_\alpha$ and $10^6$ $\tau_\alpha$, respectively. The very similar percentage of molecules outside the 95% CI for this comparison suggests no more exchange occurs between $10^5$ and$10^6$ $\tau_\alpha$ than for times shorter than $10^5$ $\tau_\alpha$.

To supplement the analysis described above in a manner that both further investigates the sensitivity of this technique compared to that of the window shifting technique and assesses whether this method can reveal dynamic exchange over periods shorter than $10^5$–$10^6$ $\tau_\alpha$, data trajectories from single movies collected at 210 K for dpPDI in glycerol are also analyzed. Here, a subset of dpPDI data at 210 K that contributes to the histogram in Fig. 4 is split into 4 trajectories of 50 $\langle\tau_c\rangle$ each. Each molecule with at least 3 consecutive 50 $\langle\tau_c\rangle$ trajectories leading to well fit LD ACFs is analyzed in the manner described above. This analysis thus investigates whether the long time heterogeneity assessment method detects temporal heterogeneity for waiting times of 50 $\langle\tau_c\rangle$, or $\sim 5 \times 10^3$ $\tau_\alpha$. 431 molecules are analyzed, and it is found that 57 (13.0%) of these molecules have their slowest rotational relaxation times outside the 95% CI obtained for molecules undergoing homogeneous rotational diffusion. A subset of these molecules, from a single movie collected at 210 K, is shown in Fig. 8c. The fact that a very similar proportion of molecules is found above the 95% CI in this experiment and in the analysis of molecules experiencing longer waiting times between data collections (Fig. 8b) supports the conclusion that no more exchanges occur between $10^3$ $\tau_\alpha$ and $10^6$ $\tau_\alpha$ then occur at times shorter than $10^3$ $\tau_\alpha$.

Comparing the result of the long time heterogeneity assessment on single trajectories at 210 K to the $\sim$27% of dpPDI molecules found to be heterogeneous at this temperature using the window shifting technique demonstrates that the sensitivity to temporal heterogeneity of the window shifting technique is greater than that of the long time heterogeneity assessment. There are several reasons for this: first, the window shifting technique is a molecule specific approach rather than a population based approach; second, the lower bound set by window size (20 $\tau_c$ for the window shifting technique *vs.* 50 $\langle\tau_c\rangle$ for the long time heterogeneity technique) means the window shifting technique is sensitive to exchanges on shorter time scales. Even given the limited sensitivity of the long time heterogeneity assessment, the result obtained here is interesting, as it suggests that molecules that do not undergo detectable dynamic exchange during typical data collection and window shifting analysis are not being missed because the trajectories are not long enough. If this were the case, the long time heterogeneity assessment technique would be expected to reveal more heterogeneous molecules for long waiting times than for short waiting times, but this is not the case. Similarly, the results suggest that of the molecules experiencing exchange in the bounds investigated by the window shifting technique, the exchange time measured is not bounded by the upper limit of sensitivity of the time investigated (set by the trajectory length) but instead by the lower limit of sensitivity. As such, we conclude that the exchange times obtained with the window shifting analyses are upper bounds on actual exchange and persistence times.

While our conclusions on average relaxation time and breadth of relaxation times of tbPDI in glycerol near $T_g$ are in close agreement with those of Zondervan *et al.*, our conclusions on temporal heterogeneity differ even though the probes used and the experiments performed are very similar.[2] We cannot exclude the possibility that the different conclusions are related to remaining differences between probes employed (tbPDI *vs.* dpPDI for the long time heterogeneity assessment) or experiments and analysis performed. Given the similarity between probes and experiments, however, we suggest that the different conclusions are due chiefly to the different sample preparation techniques employed, with the slow cooling performed by Zondervan *et al.* likely to allow for formation of a nearly static network within the sample for which we do not find evidence.[2,5,28] Instead, our results are

View Online

Published on 26 November 2010 on http://pubs.rsc.org | doi:10.1039/C0CP01860K
Downloaded by Columbia University on 04 February 2011

consistent with the picture of supercooled glycerol as a mosaic of local and interchanging environments.

## IV. Conclusions

We presented single molecule data of three perylene dyes in glycerol, all three of which report the presence of spatially heterogeneous dynamics in supercooled glycerol despite the fact that these probes are large and slow compared to glycerol molecules. For all three probes, the temperature dependence of the median rotational relaxation times mirrors the temperature dependence of the glycerol viscosity according to the DSE equation. As expected, the obtained hydrodynamic volumes depend on the probe. Unexpectedly, hydrodynamic volume is found not to scale with the size or mass of the fluorophore but instead depends strongly on the polarity and hydrogen bonding ability of the fluorophore, with tbPDI being the largest, least polar, and most quickly rotating of the three dyes studied. The distribution of single molecule $\tau_c$ values for all three dyes is qualitatively similar, with none of the distributions displaying the long time tail observed previously for rubrene in glycerol.[3] However, the distribution of rotational relaxation times becomes wider as an inverse function of the extracted probe hydrodynamic volume. For dpPDI and dapPDI, which have similar hydrodynamic volumes, there is only a small difference in distribution width, while for tbPDI, with a significantly smaller hydrodynamic volume, the distribution is much wider. Taken together with results for rubrene in glycerol, this suggests that probe molecules that rotate more quickly report a greater breadth of spatially heterogeneous dynamics in supercooled glycerol than do those that rotate slowly. Given that probe rotational relaxation time distribution breadth appears closely linked to probe rotational correlation time but not to probe molecular size for the probes used in this study implies that temporal averaging by the probe is more important in setting the breadth of reported spatially heterogeneous dynamics than is spatial averaging. For this to be the case requires that at least some dynamic exchange occurs on time scales similar to those required for probe rotation. While distribution width is found to vary with particular perylene probe, no evidence is found for significant changes in distribution shape or width for the PDI probes as a function of temperature. Similarly, the window shifting technique shows only small changes in the proportion of heterogeneous molecules as a function of temperature for a given probe compared to the difference in proportion of heterogeneous molecules found between tbPDI and the other two probes studied. Additionally, no significant changes in average exchange and persistence times relative to probe correlation time for a given probe as a function of temperature are noted. Long time heterogeneity assessment suggests, consistent with the window shifting analysis, that temporal heterogeneity exists in supercooled glycerol. The similarity in results obtained for such experiments that access exchanges on time scales of $\sim 10^3$–$10^4$ $\tau_\alpha$ and $\sim 10^5$–$10^6$ $\tau_\alpha$ is consistent with exchange primarily occurring on time scales $\leq 10^3$–$10^4$ $\tau_\alpha$. We conclude that the window shifting analysis captures a subset of dynamic exchanges, and those that are not reflected in such analysis occur on faster time scales; thus, we conclude that reported values of exchange and persistence times are upper bounds on those quantities.

## Acknowledgements

This research was supported by the National Science Foundation under grant numbers CHE 0744322 and DGE 0801530.

## References

1 L. A. Deschenes and D. A. V. Bout, *J. Phys. Chem. B*, 2002, **106**, 11438–11445.
2 R. Zondervan, F. Kulzer, G. C. G. Berkhout and M. Orrit, *Proc. Natl. Acad. Sci. U. S. A.*, 2007, **104**, 12628–12633.
3 S. A. Mackowiak, T. K. Herman and L. J. Kaufman, *J. Chem. Phys.*, 2009, **131**, 244513.
4 X. Y. Xia and P. G. Wolynes, *Phys. Rev. Lett.*, 2001, **86**, 5526–5529; G. Adam and J. H. Gibbs, *J. Chem. Phys.*, 1965, **43**, 139–146; J. P. Bouchaud and G. Biroli, *J. Chem. Phys.*, 2004, **121**, 7347–7354.
5 R. Zondervan, T. Xia, H. van der Meer, C. Storm, F. Kulzer, W. van Saarloos and M. Orrit, *Proc. Natl. Acad. Sci. U. S. A.*, 2008, **105**, 4993–4998.
6 T. Xia, L. T. Xiao and M. Orrit, *J. Phys. Chem. B*, 2009, **113**, 15724–15729.
7 M. T. Cicerone and M. D. Ediger, *J. Chem. Phys.*, 1996, **104**, 7210–7218; M. T. Cicerone, F. R. Blackburn and M. D. Ediger, *J. Chem. Phys.*, 1995, **102**, 471–479; M. Yang and R. Richert, *Chem. Phys.*, 2002, **284**, 103–114; C. Y. Wang and M. D. Ediger, *J. Phys. Chem. B*, 1999, **103**, 4177–4184; G. Heuberger and H. Sillescu, *J. Phys. Chem.*, 1996, **100**, 15255–15260; B. A. Kowert, K. T. Sobush, C. F. Fuqua, C. L. Mapes, J. B. Jones and J. A. Zahm, *J. Phys. Chem. A*, 2003, **107**, 4790–4795.
8 M. T. Cicerone and M. D. Ediger, *J. Chem. Phys.*, 1995, **103**, 5684–5692; F. R. Blackburn, C. Y. Wang and M. D. Ediger, *J. Phys. Chem.*, 1996, **100**, 18249–18257; F. R. Blackburn, M. T. Cicerone, G. Hietpas, P. A. Wagner and M. D. Ediger, *J. Non-Cryst. Solids*, 1994, **172**, 256–264; J. R. Rajian and E. L. Quitevis, *J. Chem. Phys.*, 2007, **126**, 224506; F. Qi, T. El Goresy, R. Bohmer, A. Doss, G. Diezemann, G. Hinze, H. Sillescu, T. Blochowicz, C. Gainaru, E. Rossler and H. Zimmermann, *J. Chem. Phys.*, 2003, **118**, 7431–7438; I. Chang and H. Sillescu, *J. Phys. Chem. B*, 1997, **101**, 8794–8801.
9 L. M. Wang and R. Richert, *J. Chem. Phys.*, 2004, **120**, 11082–11089.
10 W. Huang and R. Richert, *Philos. Mag.*, 2007, **87**, 371–382.
11 T. K. Herman, S. A. Mackowiak and L. J. Kaufman, *Rev. Sci. Instrum.*, 2009, **80**, 016107.
12 M. F. Gelin and D. S. Kosov, *J. Chem. Phys.*, 2006, **125**, 054708; G. Hinze, G. Diezemann and T. Basche, *Phys. Rev. Lett.*, 2004, **93**, 203001.
13 C. Y. J. Wei, Y. H. Kim, R. K. Darst, P. J. Rossky and D. A. V. Bout, *Phys. Rev. Lett.*, 2005, **95**, 173001.
14 C. Y. J. Wei, C. Y. Lu, Y. H. Kim and D. A. V. Bout, *J. Fluoresc.*, 2007, **17**, 797–804; C. Y. Lu and D. A. V. Bout, *J. Chem. Phys.*, 2006, **125**, 124701.
15 D. Bingemann, *Chem. Phys. Lett.*, 2006, **433**, 234–238.
16 M. S. Robbins and B. J. Hadwen, *IEEE Trans. Electron. Dev.*, 2003, **50**, 1227–1232.
17 F. Fujara, B. Geil, H. Sillescu and G. Fleischer, *Z. Phys. B: Condens. Matter*, 1992, **88**, 195–204; F. H. Stillinger and J. A. Hodgdon, *Phys. Rev. E: Stat. Phys., Plasmas, Fluids, Relat. Interdiscip. Top.*, 1994, **50**, 2064–2068; F. Stickel, E. W. Fischer and R. Richert, *J. Chem. Phys.*, 1996, **104**, 2043–2055.
18 H. Langhals, *Heterocycles*, 1995, **40**, 477–500.
19 L. B. A. Johansson and H. Langhals, *Spectrochim. Acta, Part A*, 1991, **47**, 857–861; A. Rademacher, S. Markle and H. Langhals, *Chem. Ber.*, 1982, **115**, 2927–2934.
20 K. Schroter and E. Donth, *J. Chem. Phys.*, 2000, **113**, 9101–9108.
21 D. B. Hall, K. E. Hamilton, R. D. Miller and J. M. Torkelson, *Macromolecules*, 1999, **32**, 8052–8058.

 This journal is © the Owner Societies 2011

View Online

22 L. Wu and S. R. Nagel, *Phys. Rev. B: Condens. Matter*, 1992, **46**, 11198–11200; E. W. Montroll and M. F. Shlesinger, *Proc. Natl. Acad. Sci. U. S. A.*, 1982, **79**, 3380–3383.
23 F. Alvarez, A. Alegria and J. Colmenero, *Phys. Rev. B: Condens. Matter*, 1991, **44**, 7306–7312; S. W. Provencher, *Comput. Phys. Commun.*, 1982, **27**, 213–227.
24 N. B. Olsen, T. Christensen and J. C. Dyre, *Phys. Rev. Lett.*, 2001, **86**, 1271–1274.
25 A. Schob, F. Cichos, J. Schuster and C. von Borczyskowski, *Eur. Polym. J.*, 2004, **40**, 1019–1026.
26 Y. Jung, J. P. Garrahan and D. Chandler, *J. Chem. Phys.*, 2005, **123**, 084509.
27 This estimate was made as follows. 1000 particles were assigned values matching the log normal rotational relaxation time distribution seen for dpPDI and dapPDI. Those particles were than reassigned values within that same distribution at random twice. All particles that were assigned a maximum value at least 3.0 times their minimum value were counted.
28 M. E. Mobius, T. Xia, W. van Saarloos, M. Orrit and M. van Hecke, *J. Phys. Chem. B*, **114**, 7439–7444.

Published on 26 November 2010 on http://pubs.rsc.org | doi:10.1039/C0CP01860K
Downloaded by Columbia University on 04 February 2011